IEEE Access
Multidisciplinary | Rapid Review | Open Access Journal

Received November 19, 2019, accepted December 8, 2019, date of publication December 13, 2019,
date of current version December 23, 2019.

Digital Object Identifier 10.1109/ACCESS.2019.2959333

Speed and Acceleration Control for a Two Wheel-Leg Robot Based on Distributed Dynamic Model and Whole-Body Control

YAXIAN XIN[1,2], HUI CHAI[1,2], YIBIN LI[1,2], XUEWEN RONG[1,2], (Member, IEEE), BIN LI[3], AND YUEYANG LI[4], (Member, IEEE)

[1]School of Control Science and Engineering, Shandong University, Jinan 250061, China
[2]Center for Robotics, Shandong University, Jinan 250061, China
[3]School of Mathematics and Statistics, Qilu University of Technology (Shandong Academy of Sciences), Jinan 250353, China
[4]School of Electrical Engineering, University of Jinan, Jinan 250022, China

Corresponding author: Hui Chai (ch2200@sina.com)

This work was supported in part by the National Key Research and Development Program of China under Grant 2017YFC0806505, in part by the National Natural Science Foundation of China under Grant U1613223, Grant 61703243, Grant 61973135, Grant 61973185, and Grant 91948201, in part by the Shandong Province Natural Science Foundation under Grant ZR2017MEE033, in part by the Shandong Province Key Research and Development Program, China, under Grant 2018GGX103054, and in part by the Development Plan of Youth Innovation Team in Colleges and Universities of Shandong Province under Grant 2019KJN011.

ABSTRACT The control technique for generating whole body motions on wheel-leg robot for dynamic locomotion and balance is a challenging topic. In this paper, a whole body dynamic model is built. It consisted by the torso dynamic model, the wheel-leg dynamic model and the contact force constraint between the wheels and the ground. A whole body control frame is proposed which composed by a torso motion controller, two torque solvers, a slippage predictor and an online trajectory generator. The torso controller plans the coupling wrenches between wheel-legs and torso. The torque solvers for every wheel-leg compute joint torques based on the coupling wrenches computed from the torso controller synchronously. The contact forces can be calculated by the slippage predictor based on the joint torques, then a boolean signal will be transmitted to the online trajectories generator to indicate whether the friction cone constraint will be broken. The online trajectory generator can plan reasonable acceleration trajectory with different boolean signals. The efficiency of this control frame is illustrated by several simulations in virtual simulation environment.

INDEX TERMS Wheel-leg robot, speed and acceleration control, distributed dynamic model, whole body control.

I. INTRODUCTION

Mobile robots have many modes of locomotion, the leg based [1]–[5] and the wheel based modes [6]–[8] have attracted a great deal of attention in recent years. Some legged robots show excellent performance overcoming obstacles in unstructured environments, but they spend more time to execute the complicated locomotion with low energy utilization compared with wheeled robots on flat terrain. Wheel-leg robots [9]–[11] can move smoothly, efficiently and fast on flat terrain.

The most famous two wheel-leg robot (WLR) is Handle from Boston Dynamics [12]. Handle developed primarily as a research platform for exploring highly dynamic behaviors. The WLRs are unstable and under-actuated intrinsically. The wrenches at the contact points with wheels and ground can not be controlled. So WLRs only can maintain balance dynamically in the unstable equilibrium point depend critically with robust controllers. Therefore the robust controllers should be designed to achieve stability. Hence, the traditional approaches based on position control and static stability are not suitable for high performance locomotion and balance control of WLRs any more.

The existing control methods of wheel-leg robots consist of two parts: one part is the balance control only using wheel joints based on the simplified inverted pendulum model, the other is the motion control [13], [14]. In [15] the dynamic model is built for the two wheeled platform to maintain the whole body balance. In [16] the wheel-leg robot is controlled for the upper and lower parts dividually. The WLR

The associate editor coordinating the review of this manuscript and approving it for publication was Jianyong Yao.

is separated at the kinematic level, the dynamic correlation between every part is neglected and the whole body dynamics for wheel-leg robot is almost no analyzed.

There are few papers that use the whole body force control for the motion control of WLRs. The whole body force control based on dynamic model is widely used for humanoid robots and quadruped robots which are very complex [17]–[19]. Their accurate dynamic models are too difficult to use for calculating the whole body torques instantly. So some assumptions and simplifications have been done to implement the dynamic force control. For instance, simplified the robot dynamics by neglecting the inertia tensor of the torso [20]; neglected the dynamic characteristics that combines the coriolis force, centrifugal force even gravity of legs by reducing the percentage of leg mass on the robot's total mass [21]. For WLR, in order to achieve high performance locomotion and dynamic balance control, the dynamic characteristics caused by wheel-legs can not be neglected.

In papers [22], [23], the virtual model control is adopted that each leg is considered as a virtual actuator mounted to the torso. But the virtual model control simplified legs as straightforward virtual actuators between each supporting foot and the torso's center of mass (CoM). In [24], the leg dynamics and torso dynamics is built firstly, then the dynamics of multilegged robot is built with the help of the coupling wrench between the legs and body. In order to maintain the dynamic balance of WLR, the wheels of WLR are not stationary refer to the inertial coordinate system. So the Jacobian matrix computed of the kinematics is not enough to control WLR. In order to achieve the dynamic force control of WLR, the whole body dynamics of the WLR should be modelled.

In this paper, a distributed modeling method is proposed. It presents multi-module form include torso dynamic model, wheel-leg dynamic models and the contact force model that is built to obtain the force at the contact points between the wheels and ground without the force sensors. Based on the distributed whole body model, the whole body control frame is constructed. It is consisted by one torso controller, two torque solvers, a slippage predictor and a online trajectory generator. With the whole body control frame, the forward speed, height and pitch angle for torso are controlled precisely. The main contributions of this paper are highlighted as follows:

1) Based on the distributed modeling method, the multi-module form model retains all the dynamic characteristics of whole body include the force interaction with torso and wheel-legs, wheels and ground, so it can be called whole-body model. This form is easy to expand when other limbs are added and easy to rewritten a integrated dynamic model of whole body.

2) The whole body control frame is used to determine the whole body joint torques based on the desired CoM motion of torso and the wheel-ground contact force constraint. The inertia force and inertia moment caused by the high-speed motion of wheel float base, coriolis force, centrifugal force and gravity of wheel-legs are all compensated for joint torques.

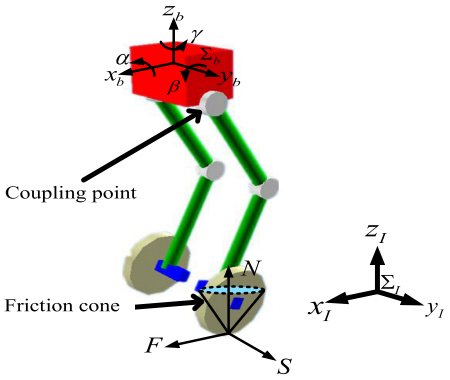

FIGURE 1. Wheel-legged robot for an example.

The paper is organized as follows. The dynamic analysis and distributed model of the WLR is built in section 2. The motion control is described in section 3. The effectiveness of the proposed approach is demonstrated through simulations and experiments in Section 4. Conclusions are given in Section 5.

II. DYNAMIC MODELING

The model of WLR is shown in Figure 1. It consists of a torso and two wheel-legs. The wheel-leg of WLR is designed with three joints which defined as the pitching hip joint, pitching knee joint and pitching wheel joint. The left part of the WLR is symmetric with its right part.

In order to let the form of the whole dynamic model suitable for control applications, a distributed dynamic modeling method is used to build the whole dynamic model of WLR. There are three major steps: build torso dynamic model, wheel-leg dynamic models and wheel-ground contact model. For the torso dynamic model, the coupling wrenches between the wheel-legs and the torso are the intuitive actuation space, the position and velocity of torso's CoM are the state space. For the wheel-leg dynamic model, the moving wheel is the floating base of each wheel-leg, the dynamic model and the friction cone constraint are developed. With the coupling wrenches, the whole dynamic model that the actuators at each joint as the actuation space can be obtained.

A. TORSO DYNAMIC MODEL

In Figure 1, Σ_I is the inertial frame of reference and Σ_b is the torso frame which attached to the geometric center of torso. In generality, we assume the two legs as two virtual actuators for torso. Expected the external forces, all the wrenches the torso receives are two contact wrenches and gravity. The ith virtual actuator can propose the force ${}^I f_i = [{}^I f_{ix}\ {}^I f_{iy}\ {}^I f_{iz}]^{\mathrm{T}}$ and the torque ${}^I n_i = [{}^I n_{ix}\ {}^I n_{iy}\ {}^I n_{iz}]^{\mathrm{T}}$ respectively. The gravity vector is ${}^I G = [0\ 0\ -m_b g]^{\mathrm{T}}$. The position of the contact point between ith leg and the torso refer to Σ_b is ${}^b P_i = [x_i\ y_i\ z_i]^{\mathrm{T}}$. The position vector and the orientation of the torso's CoM in the inertial frame are ${}^I P_b = [x_b\ y_b\ z_b]^{\mathrm{T}}$ and ${}^I \boldsymbol{\theta}_b = [\alpha\ \beta\ \gamma]^{\mathrm{T}}$ respectively. The left superscript of all the designations represents the reference frame.

The resultant wrench of the torso's CoM in Σ_I ${}^I F = [{}^I F_x \ {}^I F_y \ {}^I F_z]^{\mathrm{T}}$ and ${}^I N = [{}^I N_x \ {}^I N_y \ {}^I N_z]^{\mathrm{T}}$ can be calculated as Eqn. 1.

$$\begin{bmatrix} {}^I F \\ {}^I N \end{bmatrix} = \left[\begin{array}{c|c} D_{3\times(3\times2)} & 0_{3\times(3\times2)} \\ \hline \hat{P} & E \end{array}\right] \begin{bmatrix} {}^I f \\ {}^I n \end{bmatrix} + \begin{bmatrix} {}^I G \\ 0_{3\times1} \end{bmatrix} \tag{1}$$

where $D_{3\times(3\times2)}$ is the force distribution matrix. The $E \in \Re^{3\times3}$ is the identity matrix. ${}^I f = [{}^I f_1 \ {}^I f_2]^{\mathrm{T}}$, ${}^I n = [{}^I n_1 \ {}^I n_2]^{\mathrm{T}}$ and $\hat{P} = [\hat{P}_1 \ \hat{P}_2]$. $\hat{P}_i$ is the skew matrix with the position vector

$$\hat{P}_i = \begin{bmatrix} 0 & -z_i & y_i \\ z_i & 0 & -x_i \\ -y_i & x_i & 0 \end{bmatrix} \tag{2}$$

Based on the above-mentioned force analysis, the Newton's equation and Euler equation are shown as Eqn. 3 and Eqn. 4

$$ {}^I F = m_b {}^I \ddot{P}_b \tag{3}$$
$$ {}^I N = {}^I I_b {}^I \ddot{\boldsymbol{\theta}}_b + {}^I \dot{\boldsymbol{\theta}}_b \times {}^I I_b {}^I \dot{\boldsymbol{\theta}}_b \tag{4}$$

where ${}^I I_b$ is the inertia tensor matrix of the torso in the inertial frame.

The state-space equation of torso system can be formulated as Eqn. 6 by rewritten the Eqn. 3 and Eqn. 4. The output is as shown in Eqn. 6.

$$\dot{x} = f(x) + Bu \tag{5}$$
$$y = x \tag{6}$$

where $x = [{}^I P_b \ {}^I \boldsymbol{\theta}_b \ {}^I \dot{P}_b \ {}^I \dot{\boldsymbol{\theta}}_b{}^{\mathrm{T}}]$ is the state variable. $u = [{}^I F \ {}^I N]^{\mathrm{T}}$ is the input. With Eqn. 1, the state-space description of the system becomes:

$$\dot{x} = f\,(x) + B' u' + G_b \tag{7}$$

where $B' = B \left[\begin{array}{c|c} D_{3\times(3\times2)} & 0_{3\times(3\times2)} \\ \hline \hat{P} & I \end{array}\right]$ and $G_b = B \begin{bmatrix} {}^I G \\ 0_{3\times1} \end{bmatrix}$. $u' = [{}^I f \ {}^I n]^{\mathrm{T}}$ is the new input vector.

B. LEG DYNAMIC MODEL

As the input of the torso system, the wrenches ${}^I f_i \ {}^I n_i$ of the virtual actuators must be emulated successfully. The ${}^I f_i \ {}^I n_i$ are the output wrenches in operational space of wheel-leg systems.

In order to realize the force control in operational space used model-based control methods, the dynamic model of the leg system will be analysed. Every wheel-leg has the same joint configuration, so we just analysis the ith leg.

As shown in Figure 2, the frame Σ_0 is attached to the wheel, the frame Σ_1 and the frame Σ_2 are attached to the bottom of crus and thigh respectively. The Σ_3 is attached to the hip joint which the zero configuration is the same as Σ_2's. Limited by the configuration of the legs, only two force along the x-axis of the Σ_I and y-axis of the Σ_I and one torque around z-axis of the Σ_I can be exerted.

Different from the foot-leg, WLR's leg has a floating base which unattached to the world. The contact points on wheels

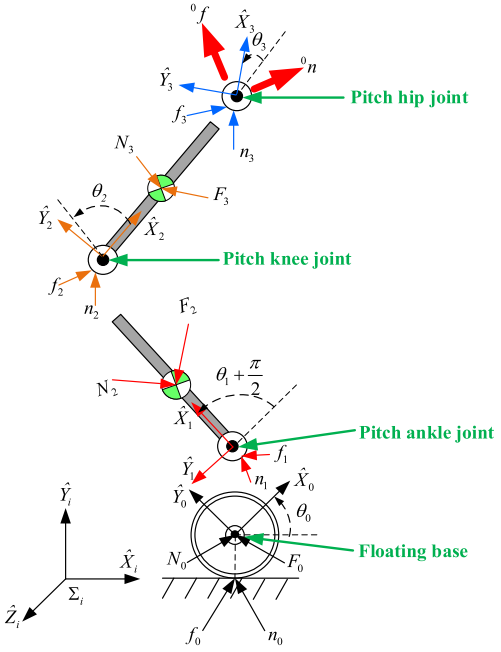

FIGURE 2. Virtual wrench.

and ground no longer still points. The interaction force and torque between cruses and wheels can drive the wheels to move.

The angular velocity vector, angular acceleration vector and linear acceleration vector of the floating base at the wheel axis are ${}^0\boldsymbol{\omega}_0 = [0 \ 0 \ \dot{\theta}_0]^{\mathrm{T}}$, ${}^0\dot{\boldsymbol{\omega}}_0 = [0 \ 0 \ \ddot{\theta}_0]^{\mathrm{T}}$ and ${}^0\dot{v}_0 = [c_0 a + s_0 g \ \ -s_0 a + c_0 g \ \ 0]^{\mathrm{T}}$ respect to Σ_0. a is the acceleration of the floating base along the $x-axis$ of Σ_I.

Using Newton-Euler recursive algorithm, the dynamic model is built as Eqn. 8

$$\boldsymbol{\tau} = M(q)\ddot{q} + C(q, \dot{q}) + G(q, \ddot{q}) + J^{\mathrm{T}} W \tag{8}$$

where $\boldsymbol{\tau} = [\tau_1 \ \tau_2 \ \tau_3]^{\mathrm{T}}$ is the joints torque vector. τ_1, τ_2 and τ_3 are the torques of ankle joint, knee joint and hip joint respectively. $q = [\theta_1 \ \theta_2 \ \theta_3]^{\mathrm{T}}$ is the joint configuration vector. $W = [{}^I f_x \ {}^I f_y \ {}^I n_z]^{\mathrm{T}}$ is the desired wrenches in wheel-leg's operational space. θ_j is the angle of Σ_j respect to Σ_{j-1}. The $M(q) \in \Re^{3\times3}$, $C(q, \dot{q}) \in \Re^{3\times1}$ and $G(q, \ddot{q}) \in \Re^{3\times1}$ are the inertia matrix, centrifugal and Coriolis matrix, gravity vector respectively. Note that the gravity vector comprises gravity compensation, the angular acceleration and linear acceleration compensation to compensation the acceleration of floating base respect to Σ_I. The detail descriptions of $M(q)$, $C(q, q)$ are $M(q) = \begin{bmatrix} M_{11} & M_{12} & 0 \\ M_{21} & M_{22} & 0 \\ 0 & 0 & 0 \end{bmatrix}$

$$M_{11} = \frac{L_1^2 m_1}{3} + L_1^2 m_2 + \frac{L_2^2 m_2}{3} + L_1 L_2 m_2 c_2$$
$$M_{12} = \frac{L_2^2 m_2}{3} + \frac{L_1 L_2 m_2 c_2}{2}$$
$$M_{21} = \frac{1}{3} L_2^2 m_2 + \frac{1}{2} L_1 L_2 m_2 c_2$$

$$M_{22} = \frac{1}{3}L_2^2 m_2 C(q, \dot{q}) = \begin{bmatrix} -L_1 L_2 m_2 s_2(\dot{\theta}_0\dot{\theta}_2 + \dot{\theta}_1\dot{\theta}_2) - L_1 L_2 m_2 s_2 \dot{\theta}_2^2/2 \\ L_1 L_2 m_2 s_2(\dot{\theta}_0 + \dot{\theta}_1)^2/2 \\ 0 \end{bmatrix}.$$

The Jacobian matrix J is

$$J = \begin{bmatrix} -L_1 s_{01} - L_2 s_{012} & -L_2 s_{012} & 0 \\ L_1 c_{01} + L_2 c_{012} & L_2 c_{012} & 0 \\ 1 & 1 & 1 \end{bmatrix} \tag{9}$$

J is a full rank matrix, so the motion of torso along x-axis, z-axis and around y-axis can be controlled independently.

When the mass of wheel-legs are big enough by contrast with torso mass, the dynamic characteristic can not be ignored. The inertia force and inertia moment of wheel-legs caused by the movement of the floating base must be compensated. The torque compensation term $\hat{G}$ is the estimated value of $G(q, \ddot{q})$ in Equation 8. It can be expressed as

$$\hat{G} = \begin{bmatrix} \hat{G}_{g0} + \hat{G}_{a0} + \hat{G}_{\ddot{\theta}0} \\ \hat{G}_{g1} + \hat{G}_{a1} + \hat{G}_{\ddot{\theta}1} \\ 0 \end{bmatrix} \tag{10}$$

where $\hat{G}_{gj}$, $\hat{G}_{aj}$ and $\hat{G}_{\theta j}$ are the combines gravity compensation torque, acceleration compensation torque and angular acceleration compensation torque for joint j. The concrete form are:

$$\begin{aligned}
\hat{G}_{g0} &= \left(\frac{L_1 m_1 c_{01}}{2} + L_1 m_2 c_{01} + \frac{L_2 m_2 c_{012}}{2}\right) g, \\
\hat{G}_{a0} &= -\left(\frac{L_1 m_1 s_{01}}{2} + L_1 m_2 s_{01} + \frac{L_2 m_2 s_{012}}{2}\right) a, \\
\hat{G}_{\ddot{\theta}0} &= \left(\frac{L_1^2 m_1}{3} + L_1^2 m_2 + \frac{L_2^2 m_2}{3} + L_1 L_2 m_2 c_2\right) \ddot{\theta}_0, \\
\hat{G}_{g1} &= \frac{L_2 m_2 c_{012}}{2} g, \\
\hat{G}_{a2} &= -\frac{L_2 m_2 s_{012}}{2} a, \\
\hat{G}_{\ddot{\theta}1} &= \left(\frac{L_2^2 m_2}{3} + \frac{L_1 L_2 m_2 c_2}{2}\right) \ddot{\theta}_0
\end{aligned}$$

Unlike foot-leg, there are no force sensors are utilized to the contact point of wheels and ground. So the floating base contact force dynamics must be built to achieve contact force control. The force of the floating base is analyzed and the contact force is calculated. As shown in Figure 2, ${}^1\mathbf{f}_1$ is the interaction force vector between crus and wheel. Part of the reacting force of the ${}^1\mathbf{f}_1$ makes floating base roll forward or back. The other part is the interaction force ${}^I\mathbf{f}_0$ between floating base and ground. Therefore, ${}^I\mathbf{f}_0$ can be calculated without force sensors as:

$${}^I\mathbf{f}_0 = \begin{bmatrix} F \\ S \\ N \end{bmatrix} = {}^I 1 R {}^I\mathbf{f}_0 + {}^I\mathbf{F}_0 \tag{11}$$

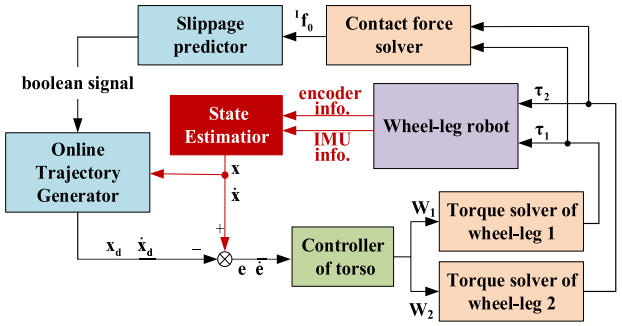

FIGURE 3. Control frame.

where ${}^I\mathbf{F}_0 = [m_0 a \; m_0 g \; 0]^{\mathrm{T}}$ is the inertia force of the floating base refer to inertia frame Σ_{I}. F and S are the friction force along x-axis and y-axis respectively. With the known nonholonomic constraints, the floating base cannot moving along z-axis. N is the support force along z-axis. The detail descriptions of F, N and S are given as follows.

$$\begin{aligned}
F &= (m_0 + m_1 + m_2)a - (L_2 m_2 s_{012}/2 + L_1 m_1 s_{01}/2 \\
&\quad + L_1 m_2 s_0 1)(\ddot{\theta}_0 + \ddot{\theta}_1) - L_2 m_2 c_{012}(\dot{\theta}_0 \\
&\quad + \dot{\theta}_1)\dot{\theta}_2 - L_2 m_2 s_{012}\ddot{\theta}_2 - (L_1 m_1 c_{01}/2 + L_1 m_2 c_{01} \\
&\quad + L_2 m_2 c_{012}/2)(\dot{\theta}_0 + \dot{\theta}_1)^2/2 - L_2 m_2 c_{012}\dot{\theta}_2^2/2 + {}^I F_x \\
S &= {}^I F_y \\
N &= (m_0 + m_1 + m_2)g + (L_2 m_2 c_{012}/2 + L_1 m_1 c_{01}/2 \\
&\quad + L_1 m_2 c_0 1)(\ddot{\theta}_0 + \ddot{\theta}_1) - L_2 m_2 s_{012}(\dot{\theta}_0 + \dot{\theta}_1)\dot{\theta}_2 \\
&\quad + L_2 m_2 c_{012}\ddot{\theta}_2/2 - (L_1 m_1 s_{01}/2 + L_1 m_2 s_{01} \\
&\quad + L_2 m_2 s_{012}/2)(\dot{\theta}_0 + \dot{\theta}_1)^2/2 - L_2 m_2 s_{012}\dot{\theta}_2^2/26958 {}^I F_z
\end{aligned}$$

III. MOTION CONTROL

In this section, a whole body torque control frame for motion control of WLR is considered. The whole control framework is shown in Figure 3.

A. TORSO CONTROLLER

For the planar motion, the torso subsystem actuated by two virtual actuators is a full drive system and the movement along $x-$axis, $z-$axis and the revolve around $y-$axis can be controlled simultaneously. In order to control the velocity along x $-$ *axis* $\dot{x}_b$ of WLR, an adaptive controller is designed refer to the literature [25]. In order to maintain the WLR's dynamic stability, the height y_b and the pitch angle β of the torso are controlled to track desired values simultaneously.

The output of the torso controller can be calculated by Eqn. 12.

$$W_d = W_{aux} + W_c \tag{12}$$

where $W_{aux} = [f_x \; f_z \; n_y]^{\mathrm{T}}$ represents the feedback wrench based on the errors of states and W_c denotes the feedforward compensation wrench based on the dynamic model of torso

in Eqn. 6.

$$W_c = \begin{bmatrix} 0 \\ 0 \\ {}^{I}I_{by}\dot{\beta}^2 \end{bmatrix} + \begin{bmatrix} 0 \\ gm_b \\ gm_b z_1 s_\beta \end{bmatrix} \tag{13}$$

where ${}^{I}I_{by}$ is the torso inertia tensor around $y-axis$.

For velocity control, the desired motion state is $\dot{x}_{bd}, \ddot{x}_{bd}$. The velocity tracking error and its time derivative are defined

$$e_x = \dot{x}_b - \dot{x}_{bd} \tag{14}$$
$$\dot{e}_x = \ddot{x}_b - \ddot{x}_{bd} \tag{15}$$

The sliding variable is

$$s = \dot{e} + \lambda e \tag{16}$$

where λ is a positive diagonal matrix. The feedback wrench is defined:

$$f_x = s + sat(s)c \tag{17}$$

where $sat(s)$ is the saturated function instead of $sign(s)$ to avoid the oscillation around the switching surface.

$$sat(s) = \begin{cases} sign(s) & if \ \ |s| > \triangle \\ \dfrac{1}{\triangle}s & otherwise \end{cases} \tag{18}$$

where $\triangle$ is the boundary layer.

c is a adaptive parameter with the parameter update law as Eqn. (19)

$$\dot{c} = \begin{cases} p\,|s| & if\ (|\hat{c}| < M) \quad or(\hat{c} = Mandp\,|s| < 0) \\ p\,|s| + \dfrac{p\,|s|\,\hat{c}^{\mathrm{T}}\hat{c}}{|\hat{c}|^2} & if(\hat{c} = Mandp\,|s| > 0) \end{cases} \tag{19}$$

where $\hat{c}$ is the estimate value of c. M is the allowable region of c.

For height control, the desired position and speed are z_{bd} and $\dot{z}_{bd}$, where $\dot{z}_{bd} = 0$. The virtual feedback force f_z can be calculated with Eqn. (20).

$$f_z = k_{pz}(z_b - z_{bd}) + k_{dz}(\dot{z}_b - \dot{z}_{bd}) \tag{20}$$

For pitch angle control, the desired angle and angular velocity are both 0. The virtual feedback torque is:

$$n_y = k_{py}(\beta - 0) + k_{dy}(\dot{\beta} - 0) \tag{21}$$

B. TORQUE SOLVER

With the desired wrench output from torso controller, the joint torques of wheel-legs will be computed using Eqn. (22) to emulate the virtual actuator.

$$\boldsymbol{\tau} = J^{\mathrm{T}}W_d + C(q, \dot{q}) + K_g\hat{G}(q, \ddot{q}) \tag{22}$$

where $K_g \in R^{3\times3}$ is the positive gain.

C. SLIPPAGE PREDICTOR

In order to prevent the slip of the wheel relative to ground, the resultant force of the tangential force and the normal force must in the friction cone shown in Figure 1. The following conditions must be satisfied.

$$\sqrt{(F^2 + S^2)} < \mu N \tag{23}$$
$$N > 0 \tag{24}$$

In this work, the contact state is 3-DOF plane contact. F and S are determined by the joint torques of hip, knee and wheel. So the joint torques must be restrained. When the desired wrenches have be determined, the joint torques and the contact forces of the wheel-legs are determined too. Only when all the joint torques are executed accurately and the ground can provide enough friction, the adaptive SMC controller can maintains the dynamic balance of the WLR.

The friction coefficient of the ground is defined μ. After the desired torques $\boldsymbol{\tau}$ in Eqn. (22) has been calculated and delivered to the *slippage predictor*. Without consideration the lateral friction S between the wheel and the ground, the friction force F and the support force N at the this moment are calculated with Eqn. (11). The friction cone constraint in Eqn. (23) becomes the following bilateral constraint as shown in Eqn. (25).

$$-\mu N \le F \le \mu N \tag{25}$$

It is too late when the bilateral constraint is not be satisfied. If the torques not be changed, the wheel will slide. If the torques are changed to avoid the slippage, the stability of WLR will be destroied because the discontinuous of the torques. In order to predict whether it will slip or not in the future times, a smaller friction coefficient $\mu - \varepsilon$ is used to construct the bilateral constraint as shown in Eqn. (26)

$$-(\mu - \varepsilon)N \le F \le (\mu - \varepsilon)N \tag{26}$$

where the value of ε is ensured based on the parameters of WLR.

A boolean signal that whether the bilateral constraint Eqn. (26) is satisfied or not will be transmitted to the *online trajectory generator*.

D. ONLINE TRAJECTORY GENERATOR

To solve the problem of slippage fundamentally, the desired trajectory along $x-axis$ should include an adaptive re-planning capability. When the mass of the legs is roughly 10% of the robot's total mass, the reacting force of the movement of legs from the contact point between the wheel and the ground as shown in Eqn. (10) can be simplified as Eqn. (27):

$${}^{I}\mathbf{f}_0 = \begin{bmatrix} F \\ S \\ N \end{bmatrix} \approx {}^{I}F = m_b{}^{I}\ddot{P}_b \tag{27}$$

From Eqn. (27), we find that the acceleration along x axis of torso is positive linearly relationship with the friction F.

After known the target velocity v_{target}, a quintic spline interpolation is projected as the desired velocity which can guarantee the smooth desired acceleration. When the boolean signal from *slippage predictor* is 0, the desired velocity and acceleration are the reference velocity and acceleration. When the boolean signal is 1 at time t, the acceleration $\ddot{x}_b(t)$ is assigned to $\ddot{x}_{bmax}$ and the desired velocity and acceleration would re-planed. Before the Eqn. (28) is satisfied, the reference acceleration is equal to $\ddot{x}_{bmax}$, the reference velocity is gained by integrate the $\ddot{x}_{bmax}$. Otherwise, decelerating phase is start to plan.

$$\frac{2(v_{target} - \dot{x}_b(t))}{T_{para}} \leq \ddot{x}_{bmax} \tag{28}$$

where $\dot{x}_b(t)$ is the velocity at time t. T_{para} is a time parameter, the bigger of the value of T_{para}, the longer and better stability of the decelerating phase.

In the decelerating phase, the reference acceleration is planed as Eqn. (29).

$$\ddot{x}_{br} = \ddot{x}_{bmax} - \frac{\ddot{x}_{bmax}}{T_{para}} t_{dece} \tag{29}$$

where the t_{dece} is the time from the start of decelerating phase to the present instant.

In order to balance the time-varied inertia force caused by the varying acceleration along $x - axis$, the relative position of the center of mass(CoM) of torso and the contact point between the wheel and the ground along $x - axis$ is not equal to 0 m. There is a constraint relationship between $\ddot{x}_b$ and y_b as shown in Equation because of the limited workspace of the leg.

$$\sqrt[2]{\left(\frac{\ddot{x}_b y_b}{g}\right)^2 + y_b^2} \leq L_{max} \tag{30}$$

When the $\ddot{x}_b$ is big enough, the desired value of y_b should be re-planed.

The flowchart of slippage predictor and online trajectory generator is shown in Figure 4.

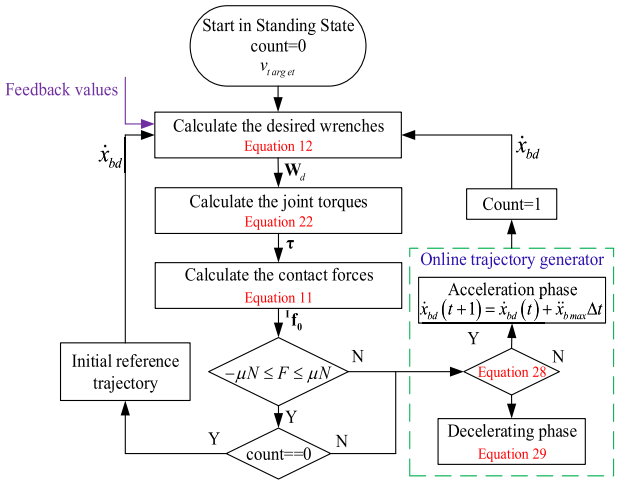

FIGURE 4. The flow diagram of slippage predictor and online trajectory generator.

IV. SIMULATIONS

In order to prove the effective of the control framework, a wheel-leg robot is built in Webots 8.4.0 as shown in Figure 7. Two simulations are implemented by co-simulation between Webots 8.4.0 and Visual Studio 2017. The controller frequency is 1000Hz. Even though the model built in Webots is 3D, only sagittal plane movement is presented for each example by divided the coupling wrench W_d to the left wheel-leg and the right wheel-leg. There are encoders at every joint, an inertial measurement unit(IMU) mounted on the CoM of torso, and a 3-axis accelerometers on the below of every calf. The mass of torso is 40kg. The mass of wheel is 2kg. The mass of crus and thigh are both 1kg. The length, width and height of torso are 0.3m, 0.2m and 0.2m respectively. The radius of wheel is 0.15m. The length and radius of crus and thigh are both 0.5m and 0.03m respectively. A video recording of the simulations can be found in https://youtu.be/VdKHIszprLw.

Two sets of simulations are presented in this section. The first one is velocity control and the second one is slippage control.

A. VELOCITY CONTROL

The control objective is to regulate the forward speed of the CoM with respect to the reference velocity expressed in the world frame. The vertical position of the CoM and the pitch angle of the torso are controlled around a constant value to maintain the balance simultaneously.

The reference velocity is given by two continuous time-varying quintic spline interpolation. The first segment is the quintic spline interpolation from $0m/s$ to $5m/s$ spending 3 seconds. The second segment is the quintic spline interpolation from $5m/s$ to $0m/s$ spending 3 seconds. The acceleration alone $x - axis$ reaches its maximum $2.5m/s^2$ when 1.5 seconds and 4.5 seconds. The constant values of the height of CoM and the pitch angle of the torso are $1.2648m$ and $0rad$ respectively. The 2D view of attitude change of the WLR in the acceleration and deceleration process is shown in Figure 5. The snapshoot is shown in Figure 6. In the acceleration process, the CoM of the WLR is on the front of the supporting point and in the deceleration process, the CoM of the WLR is in the rear of the supporting point to maintain the dynamic stability. The whole WLR with torso and legs can maintain the force balance all the time.

The torso controller is composed of Eqn. (17), Eqn. (20) and Eqn. (21). After the f_x, f_z and n_y are known, the torque resolver based on Eqn. (22) of left leg and right leg are used to solve all the joint toques. The tracking performance of horizontal velocity, height and the pitch angle of torso are shown in Figure 8, Figure 10 and Figure 11. They are clearly indicate that the controller can maintain excellent trajectory tracking and the balance control simultaneously.

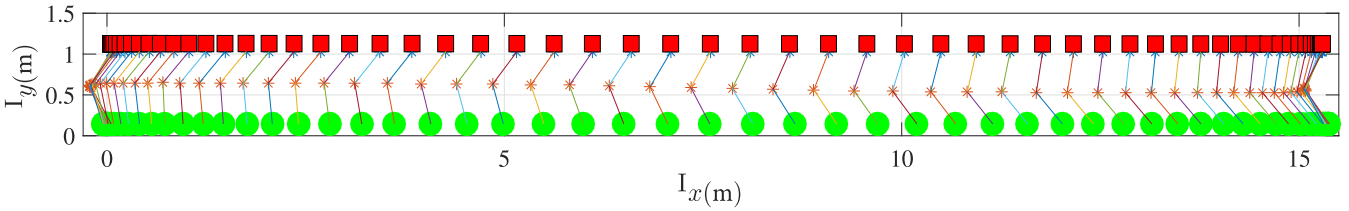

FIGURE 5. The side view of the WLR.

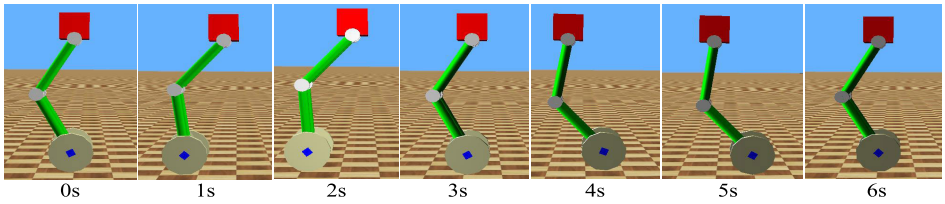

FIGURE 6. The snapshoot of the velocity tracking simulation.

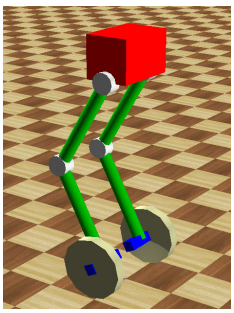

FIGURE 7. The model in the Webots.

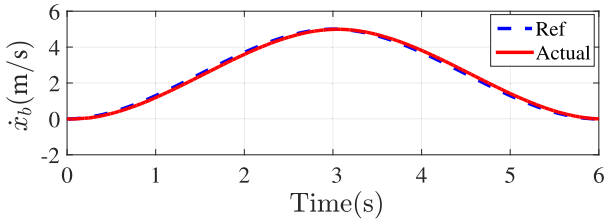

FIGURE 8. Horizontal speed control.

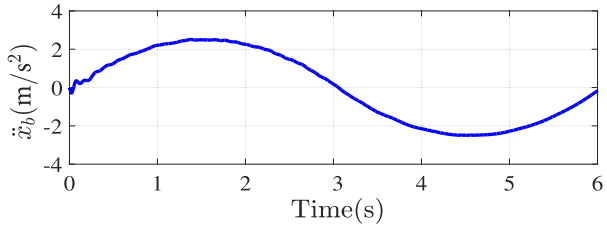

FIGURE 9. Horizontal accelerate.

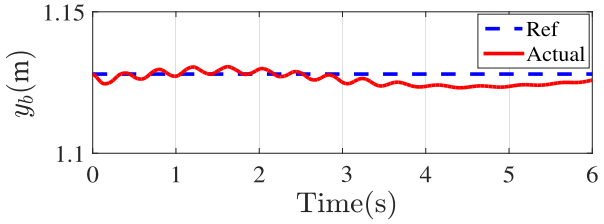

FIGURE 10. Torso height control.

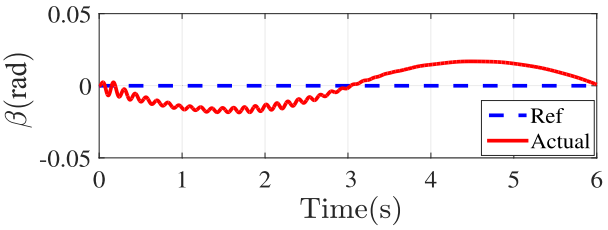

FIGURE 11. Torso pitch angle control.

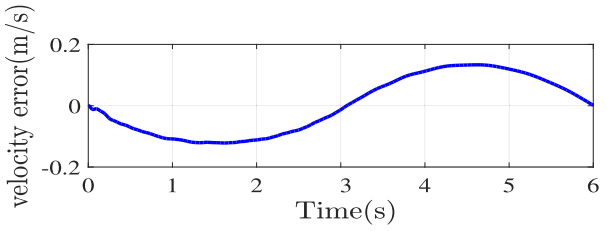

FIGURE 12. Horizontal velocity error.

As Figure 12 shows, the tracking error of horizontal velocity is changing with the change of the accelerate. After many times of simulations, we find that the bigger the accelerate is, the bigger the error is. At 1.5 seconds and 4.5 seconds, the error are $-0.1204m/s$ and $0.1328m/s$ respectively. The velocity error never account for more than 2.656% of the reference velocity. The effective control of the torso's height and pitch (Figure 11 and Figure 13) can ensure the stability of WLR. The tracking error of height is from $-0.002573m$ to $0.00484m$ and the biggest error is $4.84mm$(Figure 13). The tracking error of pitch is from $-0.0184rad$ to $0.0169rad$ and the biggest error

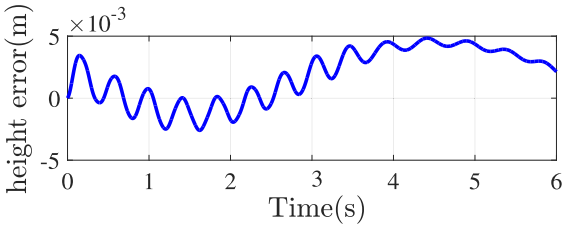

FIGURE 13. Torso height error.

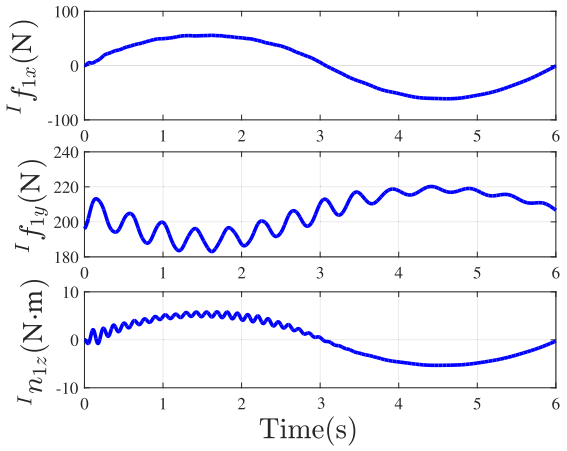

FIGURE 14. The resultant wrench of torso.

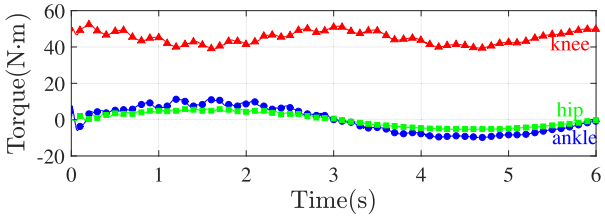

FIGURE 15. The joints torque of leg.

is 0.0184*rad*. The virtual force curves of ${}^{I}f_{1x}$ ${}^{I}f_{1y}$ and the virtual torque curve of ${}^{I}n_{1z}$ are shown in Figure 14. The torques of every joint are plotted in Figure 15 to show that the knee joint's torque is fluctuating around $45N.m$, the hip joint torque and the ankle joint torque are $0N.m$ when the horizontal acceleration is zero. Figure 16 shows the power of every joint. The ankle joint motor should have larger power than knee and hip joint motors because of its high rotate speed. The power of ankle joint motor cannot be less than $300W$. $100W$ and $10W$ can satisfy the requirements of knee and hip joint motor respectively. They have guiding significance for motor selection, motor configuration and performance estimation.

B. SLIPPAGE PREDICTABLE AND ONLINE TRAJECTORY PLANNING

In this subsection, the performance of slip predictable and online trajectory planning control are demonstrated. The static friction coefficient of the ground μ is set to 0.15 to simulate the icy roads. ε is equal to 80% of μ to maintain the system has enough stability margin. The initial

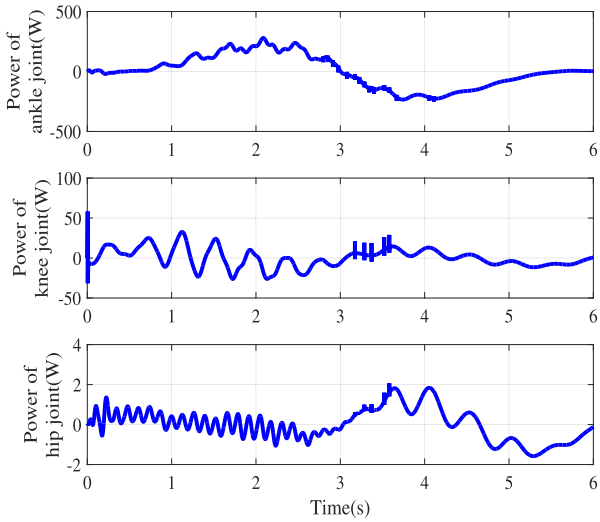

FIGURE 16. The motor power of every joint.

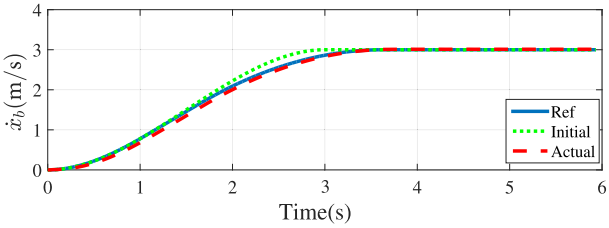

FIGURE 17. The horizontal velocity re-plan and tracking.

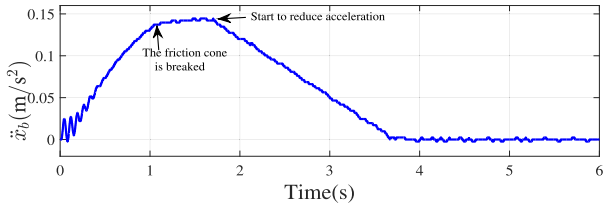

FIGURE 18. The horizontal accelerate.

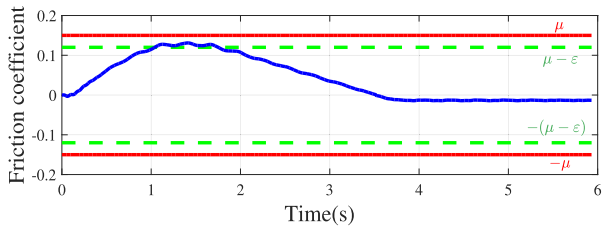

FIGURE 19. The friction coefficient.

desired trajectory, re-planning trajectory and actual trajectory of $\dot{x}_b$ are shown in Figure 17. From 0 *second* to 1.115 *second*, the reference velocity is the initial desired trajectory. At 1.115 *second* the friction cone constraint as shown in Eqn. (26) is broken, the new velocity trajectory is generated by the online trajectory generator which is the blue line in Figure 17. From 1.115 *second* to 1.719 *second*, the reference velocity is gained by integrate the $\ddot{x}_{bmax}$. At 1.719 *second*, Eqn. (28) is satisfied, the decelerating phase is start to plan

using Eqn. (29). At 3.522 *second*, the reference velocity reaches $3m/s$ and the horizontal acceleration is $0m/s^2$. The demand of friction coefficient can be calculated by F/N. Figure 19 shows it using blue line and it within the scope of the maximum friction coefficient $\mu = 0.15$.

V. CONCLUSION AND FUTURE WORK

In order to achieve the high performance locomotion and balance control of WLR, this paper has proposed a distribute whole-body dynamic modelling method and a whole-body control frame. The whole-body dynamic model is separated for the torso dynamic model, the wheel-leg floating base dynamic model and the wheel-ground contact dynamic model. The distribute dynamic model retains the dynamic correlation of the torso and the wheel-legs with the wrenches at the coupling point between the torso and wheel-legs. With the distribute dynamic method, the whole-body model is easy to expand, when adding arms or other limbs, only the new part need to be modeled. Based on the modular dynamic model, the dynamic model feedforward compensation and the adaptive state feedback constitute the torso controller in the whole-body control frame. The state feedback part include one adaptive slide mode controller to control the torso's forward speed tracking the reference trajectory, two PD controllers to maintain the height and the pitch angle of torso. The torque solvers in the whole-body control frame are constructed based on the wheel-leg model. The whole-body control frame can divide the computational load to the one torso controller and the two torque solvers. The two torque solvers running in parallel to improve the computational efficiency. This control frame allows for compliant and robust locomotion since it allows the reduction of the position gains without sacrificing tracking performance.

With the control frame, the WLR accomplish rapid acceleration and deceleration along forward direction and the dynamic balance. The maximum acceleration is $2.5m/s^2$ and the maximum error of the torso height tracking and the torso pitch tracking are $4.84mm$ and $1.05°$ respectively. The errors are small enough to verify the excellent control quality of WLR.

In the future, the control frame would be to extend to the three-dimensional movement. In order to achieve the underdrive system's whole body optimal torques, the multi-module model will be rewritten as the integrated dynamic model. Then with multi-step model prediction technique to optimize the distribution of the whole body torques.

REFERENCES

[1] Atlas. (2019). *Boston Dynamics*. [Online]. Available: https://www.bostondynamics.com/atlas
[2] Spot. (2019). *Boston Dynamics*. [Online]. Available: https://www.bostondynamics.com/spot
[3] S. Fahmi, C. Mastalli, M. Focchi, and C. Semini, "Passive whole-body control for quadruped robots: Experimental validation over challenging Terrain," *IEEE Robot. Autom. Lett.*, vol. 4, no. 3, pp. 2553–2560, Jul. 2019.
[4] T. Chen, X. Sun, F. Bergner, Z. Xu, X. Rong, and L. Zhou, "A trot and flying trot control method for quadruped robot based on optimal foot force distribution," *J. Bionic Eng.*, vol. 16, no. 4, pp. 621–632, 2019.
[5] J. Faigl and P. Cizek, "Adaptive locomotion control of hexapod walking robot for traversing rough Terrains with position feedback only," *Robot. Auton. Syst.*, vol. 116, pp. 136–147, Jun. 2019.
[6] B. Bäuml, T. Hammer, R. Wagner, O. Birbach, T. Gumpert, F. Zhi, U. Hillenbrand, S. Beer, W. Friedl, and J. Butterfass, "Agile Justin: An upgraded member of DLR's family of lightweight and torque controlled humanoids," in *Proc. IEEE Int. Conf. Robot. Automat. (ICRA)*, Hong Kong, May/Jun. 2014, pp. 2562–2563.
[7] N. Vahrenkamp, T. Asfour, and R. Dillmann, "Simultaneous grasp and motion planning: Humanoid robot ARMAR-III," *IEEE Robot. Autom. Mag.*, vol. 19, no. 2, pp. 43–57, Jun. 2012.
[8] M. K. Lee, J. Forlizzi, P. E. Rybski, F. Crabbe, W. Chung, J. Finkle, E. Glaser, and S. Kiesler, "The snackbot: Documenting the design of a robot for long-term human-robot interaction," in *Proc. 4th ACM/IEEE Int. Conf. Hum. Robot Interact.*, La Jolla, CA, USA, Jun. 2009, pp. 7–14.
[9] M. Bjelonic, C. D. Bellicoso, Y. de Viragh, D. Sako, F. D. Tresoldi, F. Jenelten, and M. Hutter, "Keep Rollin'—Whole-body motion control and planning for wheeled quadrupedal robots," *IEEE Robot. Autom. Lett.*, vol. 4, no. 2, pp. 2116–2123, Apr. 2019.
[10] Y. de Viragh, M. Bjelonic, C. D. Bellicoso, F. Jenelten, and M. Hutter, "Trajectory optimization for wheeled-legged quadrupedal robots using linearized ZMP constraints," *IEEE Robot. Autom. Lett.*, vol. 4, no. 2, pp. 1633–1640, Apr. 2019.
[11] J. A. Castano, E. M. Hoffman, A. Laurenzi, L. Muratore, M. Karnedula, and N. G. Tsagarakis, "A whole body attitude stabilizer for hybrid wheeled-legged quadruped robots," in *Proc. IEEE Int. Conf. Robot. Automat. (ICRA)*, Brisbane, QLD, Australia, May 2018, pp. 706–712.
[12] (2019). *Handle, Mobile Box Handling Robots for Logistics*. Accessed: Sep. 2, 2019. [Online]. Available: https://www.bostondynamics.com/handle
[13] Y. G. Bae and S. Jung, "Balancing control of a mobile manipulator with two wheels by an acceleration-based disturbance observer," *Int. J. Hum. Robot.*, vol. 15, no. 3, 2018, Art. no. 18500015.
[14] M. Onkol and C. Kasnakoglu, "Adaptive model predictive control of a two-wheeled robot manipulator with varying mass," *Meas. Control*, vol. 51, nos. 1–2, pp. 38–56, 2018.
[15] G. Zambella, G. Lentini, M. Garabini, G. Grioli, M. G. Catalano, A. Palleschi, L. Pallottino, A. Bicchi, A. Settimi, and D. Caporale, "Dynamic whole-body control of unstable wheeled humanoid robots," *IEEE Robot. Autom. Lett.*, vol. 4, no. 4, pp. 3489–3496, Oct. 2019.
[16] Y. Xin, X. Rong, Y. Li, B. Li, and H. Chai, "Movements and balance control of a wheel-leg robot based on uncertainty and disturbance estimation method," *IEEE Access*, vol. 7, pp. 133265–133273, 2019.
[17] S. Feng, E. Whitman, X. Xinjilefu, and C. G. Atkeson, "Optimization based full body control for the atlas robot," in *Proc. IEEE-RAS Int. Conf. Hum. Robots*, Madrid, Spain, Nov. 2014, pp. 120–127.
[18] Z. Li, S. S. Ge, and S. Liu, "Contact-force distribution optimization and control for quadruped robots using both gradient and adaptive neural networks," *IEEE Trans. Neural Netw. Learn. Syst.*, vol. 25, no. 8, pp. 1460–1473, Aug. 2014.
[19] M. Neunert, M. Stäuble, M. Giftthaler, C. D. Bellicoso, J. Carius, C. Gehring, M. Hutter, and J. Buchli, "Whole-body nonlinear model predictive control through contacts for quadrupeds," *IEEE Robot. Autom. Lett.*, vol. 3, no. 3, pp. 1458–1465, Jul. 2018.
[20] J. Di Carlo, P. M. Wensing, B. Katz, G. Bledt, and S. Kim, "Dynamic locomotion in the MIT Cheetah 3 through convex model-predictive control," in *Proc. IEEE/RSJ Int. Conf. Intell. Robots Syst. (IROS)*, Madrid, Spain, Oct. 2018, pp. 1–9.
[21] A. W. Winkler, C. Mastalli, I. Havoutis, M. Focchi, D. G. Caldwell, and C. Semini, "Planning and execution of dynamic whole-body locomotion for a hydraulic quadruped on challenging Terrain," in *Proc. IEEE Int. Conf. Robot. Automat. (ICRA)*, Seattle, WA, USA, May 2015, pp. 5148–5154.
[22] J. Pratt, A. Torres, P. Dilworth, and G. Pratt, "Virtual actuator control," in *Proc. IEEE/RSJ Int. Conf. Intell. Robots Syst.*, Osaka, Japan, Nov. 1996, pp. 1219–1226.
[23] J. Pratt, C. Chew, A. Torres, P. Dilworth, and G. Pratt, "Virtual model control: An intuitive approach for bipedal locomotion," *Int. J. Robot. Res.*, vol. 20, no. 2, pp. 129–143, 2001.
[24] Z. Li, S. Xiao, S. S. Ge, and H. Su, "Constrained multilegged robot system modeling and fuzzy control with uncertain kinematics and dynamics incorporating foot force optimization," *IEEE Trans. Syst., Man, Cybern., Syst.*, vol. 46, no. 1, pp. 1–15, Jan. 2016.

[25] S. Klecker and P. W. Plapper, "Adaptive SMC for trajectory tracking in freeform grinding," in *Proc. IEEE Int. Conf. Ind. Inform.*, Poitiers, France, Jul. 2016, pp. 196–201.

YAXIAN XIN was born in Jinan, Shandong, China, in 1990. She received the B.S. degree from Qufu Normal University, in 2014, and the M.S. degree from the Qilu University of Technology, in 2017. She is currently pursuing the Ph.D. degree with Shandong University, China. Her research interests include intelligent control and robotics.

HUI CHAI received the bachelor's, master's, and Ph.D. degrees from Shandong University, China, in 2004, 2007, and 2016, respectively. He is currently an Associate Professor with the School of Control Science and Engineering, Shandong University, China. His research interests include robotics and intelligent control.

YIBIN LI received the B.S. degree from Tianjin University, China, in 1982, the master's degree from the Shandong University of Science and Technology, China, in 1988, and the Ph.D. degree from Tianjin University, in 2006. He is currently a Professor with the School of Control Science and Engineering, Shandong University, China. His research interests include robotics, mechatronics, intelligent control, and intelligent vehicles.

XUEWEN RONG (M'10) received the B.S. and M.S. degrees from the Shandong University of Science and Technology, China, in 1996 and 1999, respectively, and the Ph.D. degree from Shandong University, China, in 2013. He is currently a Professor with the School of Control Science and Engineering, Shandong University. His research interests include bionic robotics, mechatronics, hydraulic servo transmission, and control systems.

BIN LI received the B.S., M.S., and Ph.D. degrees from Shandong University, China, in 2002, 2005, and 2012, respectively. He is currently an Associate Professor with the School of Science, Qilu University of Technology, China. He holds a postdoctoral position at Shandong University. His research interests include algorithms for neural networks and gait planning of legged robots.

YUEYANG LI (M'17) was born in Jinan, Shandong, China, in 1983. He received the B.S. and Ph.D. degrees in control theory and control engineering from Shandong University, China, in 2006 and 2011, respectively. In 2014, he was a Visiting Scholar with the Center for Robotics, Shandong University. In 2015, he was a Visiting Scholar with the Institute for Automatic Control and Complex Systems, University of Duisburg-Essen, Germany. He is currently an Associate Professor with the School of Electrical Engineering, University of Jinan, China. His main research interests include fault detection for time-varying systems, robust filtering for stochastic systems, and their applications to robotics and multidimensional systems.